American Mineralogist, Volume 94, pages 942–949, 2009

X-ray diffraction and Raman spectroscopic study of clinopyroxenes with six-coordinated Si in the $Na(Mg_{0.5}Si_{0.5})Si_2O_6$-$NaAlSi_2O_6$ system

Hexiong Yang,[1,*] Jürgen Konzett,[2] Daniel J. Frost,[3] and Robert T. Downs[1]

[1]Department of Geosciences, University of Arizona, 1040 East 4th Street, Tucson, Arizona 85721-0077, U.S.A.
[2]Institut für Mineralogie und Petrographie, Universität Innsbruck, Innrain 52, A-6020 Innsbruck, Austria
[3]Bayerisches Geoinstitut, Universität Bayreuth, Universitätsstrasse 30, D-95447 Bayreuth, Germany

Abstract

Five clinopyroxenes containing various amounts of six-coordinated Si (^{VI}Si) in the $Na(Mg_{0.5}Si_{0.5})Si_2O_6$ (NaPx)-$NaAlSi_2O_6$ (jadeite) system have been synthesized at 15 GPa and 1600 °C and their structures studied with single-crystal X-ray diffraction and Raman spectroscopy. The results show that clinopyroxenes with $^{VI}Si \leq 0.33$ atoms per formula unit (apfu) possess *C*2/*c* symmetry, whereas those with $^{VI}Si \geq 0.45$ apfu crystallize with *P*2/*n* symmetry. There is an obvious discontinuity in the unit-cell parameters *a*, β, and *V* as the ^{VI}Si content increases from 0.33 to 0.45 apfu, suggesting that the *C*2/*c*-*P*2/*n* transition is first-order in character, rather than tricritical as reported for the transition from jadeite/diopside/augite to omphacite. The Mg and ^{VI}Si cations in the *P*2/*n* structure are completely ordered into two nonequivalent octahedral sites, M1 and M1(1), respectively, with M1 being appreciably more distorted than M1(1). With increasing mean <M1-O> distance, the mean tetrahedral <Si-O> distance increases, whereas the O3-O3-O3 angle of the tetrahedral chain decreases systematically, consistent with the structural variation trends found in the jadeite-diopside system. A comparison of the Raman spectra reveals that the *C*2/*c*-*P*2/*n* transition is characterized by the splitting of many Raman bands in *C*2/*c* clinopyroxenes into doublets in *P*2/*n*, and such splitting becomes more pronounced with increasing ^{VI}Si. For *C*2/*c* clinopyroxenes, all Raman bands become progressively broader with the increased substitution of $(Si^{4+} + Mg^{2+})$ for Al^{3+}. In addition, several new Raman bands, attributable to the presence of ^{VI}Si, are observed. Together with previous data, we suggest that the maximum ^{VI}Si content allowed for an Mg/Al dominated octahedral site is close to ~35%, above which ^{VI}Si and Mg/Al are likely to be ordered into distinct sites.

Keywords: Clinopyroxenes, six-coordinated silicon, X-ray structure refinement, Raman spectroscopy, phase transformation

Introduction

Research on materials containing six-coordinated silicon (^{VI}Si) plays a key role in our efforts to understand the composition and structure of the Earth's interior and to synthesize new materials with novel properties (e.g., Finger and Hazen 1991). Clinopyroxenes, one of the most important rock-forming minerals in the Earth's crust and upper mantle, had long been assumed to contain tetrahedrally coordinated Si only. Recent high-pressure experiments, however, have revealed the capability of clinopyroxenes to accommodate ^{VI}Si (Angel et al. 1988; Yang and Konzett 2005), suggesting that their stability field may be expanded to higher pressures than previously assumed (Angel et al. 1988; Gasparik 1989). Moreover, an inclusion in diamond with the composition $(Na_{0.16}Mg_{0.84})(Mg_{0.92}Si_{0.08})Si_2O_6$ was recently found in a kimberlite in China (Wang and Sueno 1996), suggesting that parts of the Earth's upper mantle may be characterized by an excess of Na with respect to Al in the bulk, a situation not known to prevail in peridotitic portions of the upper mantle regularly sampled by xenoliths. A review of supersilicic (Si > 2 apfu) clinopyroxenes was presented by Day and Mulcahy (2007).

Two clinopyroxenes containing ^{VI}Si have been examined with single-crystal X-ray diffraction prior to this study. One of them is $Na(Mg_{0.5}Si_{0.5})Si_2O_6$ clinopyroxene (NaPx) synthesized at 15 GPa and 1600 °C (Angel et al. 1988). This high-pressure phase possesses *P*2/*n* symmetry and is topologically analogous to ordered *P*2/*n* omphacites, with Mg and Si occupying two distinct M1 octahedral sites. Yang and Konzett (2005) reported a *C*2/*c* $(Ca_{0.36}Na_{0.56}Mg_{0.08})(Mg_{0.73}Si_{0.27})Si_2O_6$ clinopyroxene synthesized at 15 GPa and 1600 °C, which is isostructural with diopside/jadeite and shows no detectable ordering between Mg^{2+} and Si^{4+} in the M1 octahedral site. Several questions then arise regarding the relative stabilities of *P*2/*n* and *C*2/*c* clinopyroxenes with respect to ^{VI}Si content. One of them is whether *C*2/*c* $(Ca_{0.36}Na_{0.56}Mg_{0.08})(Mg_{0.73}Si_{0.27})Si_2O_6$ clinopyroxene is stabilized by: (1) less ^{VI}Si (0.27 apfu) in the M1 site than that found in NaPx (0.5 apfu); (2) the substitution of a considerable amount of Ca^{2+} for Na^+ in the M2 site; or (3) the coupled effects of both factors. Another question is how much ^{VI}Si the *C*2/*c* structure can accommodate.

Structural relations between *C*2/*c* jadeite/diopside/augite and *P*2/*n* omphacite have been investigated extensively because of

* E-mail: hyang@u.arizona.edu

the common occurrence of omphacite in high-pressure eclogite and blueschist facies rocks (e.g., Rossi et al. 1983; Carpenter et al. 1990a, 1990b; Boffa Ballaran and Domeneghetti 1996; Boffa Ballaran et al. 1998a, 1998b; Pavese et al. 2000; Katerinopoulou et al. 2007) and an excellent review on this subject has been given by Rossi (1983). Figure 1 illustrates the structural differences between *C*2/*c* and *P*2/*n* pyroxenes. It is generally agreed that the *C*2/*c*-to-*P*2/*n* transition in clinopyroxenes is tricritical in character and results from coupled cation substitutions: $Na^{+} + Al^{3+}$ (or Fe^{3+}) ↔ $Ca^{2+} + Mg^{2+}$ (or Fe^{2+}). These cations are distributed over two distinct sets of sites in the *P*2/*n* omphacite structure. On the one hand, Mg^{2+} (Fe^{2+}) and Al^{3+} (Fe^{3+}) are ordered between two nonequivalent octahedral sites, M1 and M1(1), respectively (after the site nomenclature of Matsumoto et al. 1975 and Curtis et al. 1975), which alternate along the *c* axis through edge-sharing. On the other hand, Na^{+} and Ca^{2+} are preferentially partitioned into two eight-coordinated sites, M2 and M2(1), respectively (Fig. 1b). The degree of cation ordering between the two M2 sites is considerably less than that between the two M1 sites. For the jadeite-diopside system, *P*2/*n* omphacites generally fall between values of Na/(Na + Ca) ≈ 0.30 and 0.70, depending on the temperatures and pressures of their formation.

In this paper, we present a systematic structural study on a series of clinopyroxenes synthesized at high pressures along the $Na(Mg_{0.5}Si_{0.5})Si_2O_6$-$NaAlSi_2O_6$ join by means of single-crystal X-ray diffraction and Raman spectroscopy. Our results show that the *C*2/*c*-*P*2/*n* transition in this system takes place between ^{VI}Si = 0.33 and 0.45 apfu. It is first-order in nature and does not require the coupled substitutions between the M1 and M2 cations.

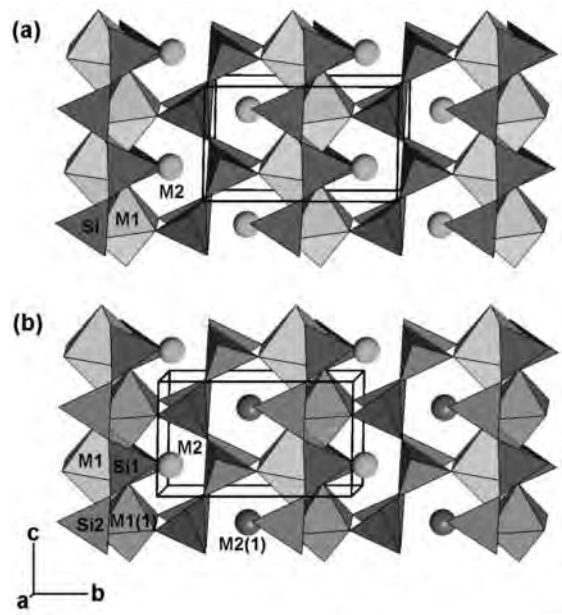

FIGURE 1. Structural comparison between (**a**) *C*2/*c* and (**b**) *P*2/*n* clinopyroxenes.

EXPERIMENTAL METHODS

Five samples in the $Na(Mg_{0.5}Si_{0.5})Si_2O_6$-$NaAlSi_2O_6$ system were synthesized at 15 GPa and 1600 °C with a 1000-ton multi-anvil device at the Bavarian Research Institute of Experimental Geochemistry and Geophysics. The starting materials were prepared by mixing appropriate amounts of high purity (≥99.99%) oxides and carbonates in ethanol and stepwise decarbonation. For higher reactivity, Al was added as γ-Al_2O_3. After storage at 150 °C for at least 72 h, all starting materials were welded into 1.6 mm outer diameter Pt_{100}-capsules with a length not exceeding 2.7 mm. All experiments were run in 14/8 multi anvil assemblages (14 mm edge-length of octahedron and 8 mm truncation of WC-cubes) with precast MgO-based ceramic and $LaCrO_3$-furnace combined with pyrophyllite gaskets. Temperatures were measured with W3%Re-W25%Re thermocouples, and both pressure and temperature were computer-controlled during the entire duration of the runs. After run durations of 17 to 32 h, the experiments were quenched by shutting off the power to the transformer with subsequent pressure release. After removal from the assembly, the capsules were embedded in epoxy resin and ground to expose the experimental charge for electron microprobe analysis, micro-Raman spectroscopy and extraction of crystals for X-ray diffraction analyses.

The compositions of all samples (Table 1) were analyzed with a JEOL 8100 Superprobe in the wavelength dispersive analytical mode with analytical conditions of 15 kV acceleration voltage and 10 nA beam current. Measurement times on peaks and backgrounds of the X-ray lines of 20 and 10 s, respectively, were chosen. The following standards were used: Si, natural α-quartz; Al, synthetic corundum; Mg, natural diopside; Na, natural jadeite. All analyses were on-line corrected using the PRZ correction procedure.

Raman spectra were recorded from randomly oriented single crystals exposed at the polished surface of the experimental charges. The samples were excited by the 488 or 514 nm emission line of an Ar-ion laser through a 100× objective (numerical aperture 0.9) using a laser power of 5–7 mW and a laser spot diameter of ~1 µm. The spectral resolution, experimentally determined by measuring the full-width at half maximum of the Rayleigh line, was about 1.8 cm^{-1}. The dispersed light was collected by a 1024 × 256 open electrode CCD detector with a confocal pinhole set to 1 mm. All spectra were baseline-corrected assuming linear background and deconvoluted by Gauss-Lorentz functions using the built-in spectrometer software Labspec 4. Raman shifts were calibrated by the zero-order position of the grating and the Rayleigh line of a (100) polished single-crystal silicon-wafer. The accuracy of the determined band positions is better than 0.5 cm^{-1}.

Based on optical examination and X-ray diffraction peak profiles, a nearly equi-dimensional crystal was selected from each sample and mounted on a Bruker X8 APEX2 CCD X-ray diffractometer equipped with graphite-monochromatized Mo*K*α radiation. X-ray diffraction data were collected with frame widths of 0.5° in ω and 30 s counting time per frame. All reflections were indexed on the basis of a monoclinic unit cell (Table 2). The intensity data were corrected for X-ray absorption using the Bruker program SADABS. Although observed systematic absences of reflections indicated the possible space groups *P*2/*n* or *Pn* for samples J1 and J2, and *C*2/*c* or *Cc* for the other three samples, the E-value statistics of the X-ray intensity data showed that all crystals are most likely centrosymmetric, which was confirmed in the subsequent structure refinements.

The initial structure models for *P*2/*n* and *C*2/*c* clinopyroxenes were taken from those reported by Angel et al. (1988) and Yang and Konzett (2005), respectively.

TABLE 1. Chemistry of clinopyroxenes with six-coordinated Si

Sample no.	J1	J2	J3	J4	J5
Run no.	B2002-2	B2006-4	B2005-4	B2005-14	B2005-12
Analysis points	14	13	18	13	15
			Oxides (wt%)		
SiO_2 (wt%)	73.74(29)	74.21(47)	69.53(64)	65.77(44)	63.34(33)
Al_2O_3		2.51(43)	7.57(1.12)	13.25(50)	18.46(38)
MgO	10.59(15)	9.33(19)	7.93(53)	5.38(24)	3.54(15)
Na_2O	14.89(10)	15.60(18)	14.91(13)	14.68(18)	15.24(13)
Total	99.21(38)	101.65(51)	99.93(32)	99.08(35)	100.58(31)
			Cation numbers normalized based on six O atoms		
Si	2.490(4)	2.448(9)	2.334(21)	2.227(11)	2.119(8)
Al	0	0.098(17)	0.299(44)	0.529(21)	0.728(15)
Mg	0.533(7)	0.459(10)	0.397(26)	0.271(12)	0.177(7)
Na	0.975(6)	0.998(9)	0.970(9)	0.964(10)	0.989(8)
Total cations no.	3.998(6)	4.003(7)	4.000(7)	3.991(9)	4.013(6)
M1 occupancy	$Mg_{0.51}Si_{0.49}$	$Mg_{0.45}Al_{0.10}Si_{0.45}$	$Mg_{0.37}Al_{0.30}Si_{0.33}$	$Mg_{0.24}Al_{0.55}Si_{0.21}$	$Mg_{0.16}Al_{0.70}Si_{0.14}$
M2 occupancy	$Na_{0.98}Mg_{0.02}$	$Na_{1.00}$	$Na_{0.97}Mg_{0.03}$	$Na_{0.97}Mg_{0.03}$	$Na_{0.99}Mg_{0.01}$

Note: The chemistry of the M1 and M2 sites were determined by normalizing the total cation numbers from electron microprobe analyses to four with a total positive charge of 12.

TABLE 2. Summary of crystal data and refinement results of clinopyroxenes with six-coordinated Si

Sample	J1	J2	J3	J4	J5
Space group	*P*2/*n* (No. 13)	*P*2/*n*	*C*2/*c* (No. 15)	*C*2/*c*	*C*2/*c*
a (Å)	9.4051(6)	9.3957(6)	9.4410(3)	9.4429(5)	9.4373(4)
b (Å)	8.6436(5)	8.6262(8)	8.6038(3)	8.5946(4)	8.5804(3)
c (Å)	5.2679(3)	5.2588(5)	5.2547(2)	5.2437(3)	5.2348(3)
β (°)	108.142(3)	108.050(5)	107.833(2)	107.741(3)	107.647(3)
V (Å^3)	406.95(6)	405.25(7)	406.32(2)	405.33(4)	403.94(3)
No. of reflections for cell refinements	960	599	1077	2045	1071
θ range for cell-refinement reflections	2.36–34.96	4.00–32.78	3.28–34.90	3.28–40.07	3.28–35.60
Z	4	4	4	4	4
ρ_{calc} (g/cm^3)	3.390	3.306	3.295	3.303	3.328
μ (mm^{-1})	1.19	1.15	1.15	1.15	1.15
θ range for data collection	2.36–34.96	2.36–34.95	3.28–34.90	3.28–34.94	3.28–34.96
No. of reflections collected	7964	7922	4068	4080	4274
No. of independent reflections	1736	1784	841	895	891
No. of reflections with $I > 2\sigma(I)$	1294	1057	707	815	819
No. of $h + k$ = odd reflections [$I > 2\sigma(I)$]	441	416	21	15	13
No. of parameters refined	94	94	48	48	48
R(int)	0.029	0.061	0.017	0.019	0.018
Final R_1 and wR_1 factors [$I > 2\sigma(I)$]	0.032, 0.083	0.041, 0.092	0.027, 0.070	0.021, 0.065	0.019, 0.061
Final R_1 and wR_1 factors (all data)	0.048, 0.091	0.087, 0.107	0.034, 0.072	0.023, 0.066	0.021, 0.062
Goodness-of-fit	1.067	1.045	1.138	1.373	1.322

All structures were refined with anisotropic displacement parameters for all atoms using SHELX97 (Sheldrick 2008). During the refinements, the chemical compositions were constrained to those determined from electron microprobe analyses. The structure refinement on sample J1 showed that Mg and Si are fully ordered at the M1 and M1(1) sites, respectively, as also observed by Angel et al. (1988). Accordingly, for sample J2, we assigned all Mg in M1 and Si in M1(1), and filled the rest of these sites with Al, so that there is 0.08 Al in M1 and 0.12 in M1(1). Final atomic coordinates and isotropic displacement parameters are listed in Table 3, anisotropic displacement parameters in Table 4, and selected bond distances and angles in Table 5.

RESULTS AND DISCUSSION

Structural variations associated with the *C*2/*c*-to-*P*2/*n* phase transition in the jadeite-NaPx system are similar to those in the jadeite (or diopside)-omphacite system, both being characterized by the splitting of each atomic site in the *C*2/*c* phase into two nonequivalent sites in the *P*2/*n* phase. In other words, three cation sites in the *C*2/*c* structure (i.e., 4-, 6-, and 8-coordinated Si, M1, and M2 sites, respectively) become six in the *P*2/*n* structure [Si1, Si2, M1, M1(1), M2, and M2(1)] (Fig. 1). However, due to the greater differences between Mg^{2+} and Si^{4+} in terms of ionic radius and charge than those between Mg^{2+} and Al^{3+}, more dramatic structural changes associated with the *C*2/*c*-*P*2/*n* transition are expected for the jadeite-NaPx system than for the jadeite (diopside)-omphacite system, particularly with respect to the modifications around the octahedral sites occupied by these cations.

As shown in Figure 2, the *C*2/*c*-*P*2/*n* transition between ^{VI}Si = 0.33 and 0.45 apfu in the jadeite-NaPx system is marked by noticeable changes in all unit-cell dimensions, especially by the discontinuities in *a*, β, and *V*. This transition is, therefore, first-order in nature, rather than tricritical, as observed for the jadeite/diopside-omphacite system (Rossi 1983; Carpenter et al. 1990a; Boffa Ballaran and Domeneghetti 1996). It is interesting to note that all unit-cell parameters of *C*2/*c* clinopyroxenes increase with increasing ^{VI}Si content, but the *a* dimension appears to decrease slightly as ^{VI}Si increases from 0.21 to 0.33 apfu. This behavior is perhaps a precursor for the onset of the phase transformation. In addition, our data lend further support to the observation that the unit-cell geometry of sodic clinopyroxenes is strongly dependent upon the chemistry of their M1 octahedral sites (Rossi et al. 1981, 1983).

Intimately correlated to the variations in the unit-cell dimensions from jadeite to NaPx is the remarkable alteration in the distortion indices of the octahedral sites, as measured by the octahedral angle variance (OAV) and quadratic elongation (OQE) (Robinson et al. 1971). These two values are essentially constant (OAV = 48 ± 1 and OQE = 1.015) for the M1 octahedron in the *C*2/*c* clinopyroxene samples (Table 5), but become 104(3) and 1.034(1), respectively, for M1, and 15(1) and 1.004(1) for M1(1) in the *P*2/*n* samples. In contrast, for the jadeite (diopside)-omphacite system, the OAV and OQE values only vary between 18 and 45 and between 1.006 and 1.014, respectively (Rossi et al. 1983). The significant changes in the distortion indices of the M1 and M1(1) octahedra in our *P*2/*n* clinopyroxenes, relative to the M1 octahedron in *C*2/*c* clinopyroxenes, are a direct consequence of the complete ordering of Mg^{2+} into M1 and Si^{4+} into M1(1). In *P*2/*n* clinopyroxenes, the M1 and M1(1) octahedra share two edges with each other to form chains parallel to *c* (Fig. 1). To maintain such a linkage, the shared edges of the comparatively large and soft M1 octahedra have to be shortened substantially to match those of the small and strongly bonded (i.e., rigid) M1(1) octahedra, causing the O1(1)-M1-O1(2) angle subtending the shared edge to deviate considerably from the ideal value of 90°. For our J1 sample, this angle is only 69.5°, compared to 84.7° for the O1(1)-M1(1)-O1(2) angle subtending the same shared edge. The corresponding O1(1)-M1-O1(2) and O1(1)-M1(1)-O1(2) angles in omphacite (Matsumoto et al. 1975; Mottana et al. 1979) are ~77.8 and ~83.3°, respectively. Coupled with these changes is a notable elongation of the M1-O1(1) and M1-O1(2) distances, as well as the M1(1)-O1(1) and M1(1)-O1(2) distances (Table 5), owing to the strong Mg^{2+}-$^{VI}Si^{4+}$ repulsion. In fact, the separation between the two adjacent cations in the octahedral chains in the J1 sample (3.115 Å) is greater than in any clinopyroxenes in the jadeite-diopside system: 3.069 Å for jadeite (McCarthy et al. 2008), 3.092 Å for diopside (Levien and Prewitt 1981), and 3.107 Å for omphacite (Mottana et al. 1979), thus accounting for the largest *c* dimension of all these pyroxenes.

To facilitate a better comparison between the *C*2/*c* and *P*2/*n*

TABLE 3. Atomic coordinates and isotropic displacement parameters

Sample		J1	J2	J3	J4	J5
M2		$Na_{0.96}Mg_{0.04}$	$Na_{1.00}$	$Na_{0.97}Mg_{0.03}$	$Na_{0.97}Mg_{0.03}$	$Na_{0.99}Mg_{0.01}$
	x	¾	¾	0	0	0
	y	0.0515(1)	0.0517(2)	0.2990(1)	0.2994(1)	0.2998(1)
	z	¼	¼	¼	¼	¼
	U_{eq}	0.0106(3)	0.0113(4)	0.0154(3)	0.0140(2)	0.0126(2)
M2(1)		$Na_{1.00}$	$Na_{1.00}$			
	x	¾	¾			
	y	0.4564(1)	0.4558(2)			
	z	¾	¾			
	U_{eq}	0.0155(3)	0.0166(5)			
M1		$Mg_{1.00}$	$Mg_{0.92}Al_{0.08}$	$Mg_{0.37}Al_{0.30}Si_{0.33}$	$Mg_{0.24}Al_{0.55}Si_{0.21}$	$Mg_{0.16}Al_{0.70}Si_{0.14}$
	x	¾	¾	0	0	0
	y	0.6547(1)	0.6550(1)	0.9048(1)	0.9051(1)	0.9056(1)
	z	¼	¼	¼	¼	¼
	U_{eq}	0.0069(3)	0.0075(4)	0.0065(2)	0.0052(3)	0.0047(3)
M1(1)		$Si_{0.98}Mg_{0.02}$	$Si_{0.88}Al_{0.12}$			
	x	¾	¾			
	y	0.8471(1)	0.8470(1)			
	z	¾	¾			
	U_{eq}	0.0052(2)	0.0056(3)			
Si1	*x*	0.0447(1)	0.0443(1)	0.2905(1)	0.2905(1)	0.2905(1)
	y	0.8485(1)	0.8480(1)	0.0925(1)	0.0928(1)	0.0930(1)
	z	0.2263(1)	0.2267(1)	0.2301(1)	0.2296(1)	0.2291(1)
	U_{eq}	0.0059(1)	0.0068(2)	0.0074(1)	0.0064(1)	0.0057(1)
Si2	*x*	0.0372(1)	0.0374(1)			
	y	0.6653(1)	0.6647(1)			
	z	0.7357(1)	0.7349(1)			
	U_{eq}	0.0060(1)	0.0073(2)			
O1(1)	*x*	0.8622(1)	0.8620(2)	0.1093(1)	0.1094(1)	0.1094(1)
	y	0.8442(1)	0.8430(2)	0.0767(1)	0.0765(1)	0.0764(1)
	z	0.1017(2)	0.1034(4)	0.1293(3)	0.1291(2)	0.1289(2)
	U_{eq}	0.0075(2)	0.0092(4)	0.0175(3)	0.0135(3)	0.0097(2)
O1(2)	*x*	0.8563(1)	0.8564(2)			
	y	0.6930(1)	0.6915(2)			
	z	0.6565(2)	0.6548(4)			
	U_{eq}	0.0073(2)	0.0086(4)			
O2(1)	*x*	0.1236(1)	0.1228(2)	0.3607(1)	0.3608(1)	0.3609(1)
	y	0.0150(1)	0.0149(2)	0.2619(1)	0.2625(1)	0.2628(1)
	z	0.3069(2)	0.3061(4)	0.2973(2)	0.2962(2)	0.2953(2)
	U_{eq}	0.0085(2)	0.0102(4)	0.0143(2)	0.0123(2)	0.0104(2)
O2(2)	*x*	0.0892(1)	0.0992(2)			
	y	0.4950(1)	0.4946(2)			
	z	0.7906(2)	0.7909(4)			
	U_{eq}	0.0109(2)	0.0114(4)			
O3(1)	*x*	0.1125(1)	0.1119(2)	0.3532(1)	0.3534(1)	0.3536(1)
	y	0.7669(1)	0.7663(2)	0.0076(1)	0.0076(1)	0.0074(1)
	z	0.0120(2)	0.0114(4)	0.0086(2)	0.0078(2)	0.0074(2)
	U_{eq}	0.0086(2)	0.0098(4)	0.0117(2)	0.0103(2)	0.0090(2)
O3(2)	*x*	0.0926(1)	0.0933(2)			
	y	0.7526(1)	0.7518(2)			
	z	0.5067(2)	0.5059(4)			
	U_{eq}	0.0084(2)	0.0097(4)			

TABLE 4. Atomic displacement parameters (Å^2) of clinopyroxenes with six-coordinated Si

	U_{11}	U_{22}	U_{33}	U_{12}	U_{13}	U_{23}
Sample J1						
M2	0.0122(6)	0.0089(5)	0.0086(5)	0	0.0003(4)	0
M2(1)	0.0206(7)	0.0089(5)	0.0124(5)	0	−0.0016(5)	0
M1	0.0070(4)	0.0064(4)	0.0070(4)	0	0.0017(3)	0
M1(1)	0.0051(3)	0.0046(3)	0.0057(3)	0	0.0016(2)	0
Si1	0.0058(2)	0.0057(2)	0.0060(2)	−0.0004(2)	0.0016(2)	−0.0002(1)
Si2	0.0057(2)	0.0059(2)	0.0063(2)	0.0003(2)	0.0018(2)	0.0005(1)
O1(1)	0.0059(5)	0.0088(5)	0.0069(5)	−0.0006(4)	0.0009(4)	−0.0006(4)
O1(2)	0.0055(5)	0.0083(5)	0.0083(5)	0.0006(4)	0.0024(4)	−0.0003(4)
O2(1)	0.0099(6)	0.0064(5)	0.0093(5)	−0.0020(4)	0.0033(5)	−0.0003(4)
O2(2)	0.0119(6)	0.0087(5)	0.0120(5)	0.0018(5)	0.0037(5)	0.0004(4)
O3(1)	0.0076(6)	0.0100(5)	0.0081(5)	−0.0001(4)	0.0023(5)	−0.0020(4)
O3(2)	0.0084(6)	0.0096(5)	0.0074(5)	−0.0012(4)	0.0027(4)	0.0018(4)
Sample J2						
M2	0.0147(7)	0.0069(8)	0.0102(9)	0	0.0010(6)	0
M2(1)	0.0226(9)	0.0082(8)	0.0136(1)	0	−0.0021(7)	0
M1	0.0073(5)	0.0077(6)	0.0076(7)	0	0.0021(5)	0
M1(1)	0.0065(4)	0.0053(5)	0.0053(5)	0	0.0020(3)	0
Si1	0.0072(3)	0.0068(3)	0.0064(3)	−0.0004(2)	0.0018(2)	−0.0004(3)
Si2	0.0072(3)	0.0078(3)	0.0069(3)	0.0002(2)	0.0021(2)	0.0005(3)
O1(1)	0.0064(7)	0.0108(8)	0.0095(9)	0.0007(6)	0.0013(6)	−0.0013(7)
O1(2)	0.0063(7)	0.0079(8)	0.0109(9)	0.0013(6)	0.0017(6)	0.0012(7)
O2(1)	0.0103(7)	0.0088(8)	0.0109(9)	−0.0017(6)	0.0024(7)	0.0000(7)
O2(2)	0.0135(8)	0.0089(8)	0.0115(9)	0.0008(6)	0.0034(7)	0.0011(7)
O3(1)	0.0089(7)	0.0123(9)	0.0085(9)	0.0008(6)	0.0033(7)	−0.0015(7)
O3(2)	0.0085(7)	0.0111(8)	0.0087(9)	0.0004(6)	0.0016(7)	0.0036(7)
Sample J3						
M2	0.0201(5)	0.0111(4)	0.0105(5)	0	−0.0017(4)	0
M1	0.0069(3)	0.0073(3)	0.0047(3)	0	0.0011(2)	0
Si	0.0070(2)	0.0098(2)	0.0051(2)	0.0001(1)	0.0013(1)	−0.0009(1)
O1	0.0074(4)	0.0233(6)	0.0201(6)	0.0009(4)	0.0014(5)	−0.0117(5)
O2	0.0209(5)	0.0108(4)	0.0111(5)	−0.0012(4)	0.0047(4)	−0.0007(4)
O3	0.0121(5)	0.0168(5)	0.0063(5)	0.0039(4)	0.0030(4)	−0.0015(4)
Sample J4						
M2	0.0178(4)	0.0097(4)	0.0110(4)	0	−0.0008(3)	0
M1	0.0049(3)	0.0056(3)	0.0048(3)	0	0.0012(2)	0
Si	0.0056(2)	0.0077(2)	0.0059(2)	−0.0001(1)	0.0016(1)	−0.0008(1)
O1	0.0058(3)	0.0171(4)	0.0169(4)	0.0007(3)	0.0023(3)	−0.0065(3)
O2	0.0165(4)	0.0089(3)	0.0114(4)	−0.0017(3)	0.0039(3)	−0.0008(3)
O3	0.0095(3)	0.0143(4)	0.0072(3)	0.0021(3)	0.0026(3)	−0.0019(3)
Sample J5						
M2	0.0158(4)	0.0087(3)	0.0102(4)	0	−0.0010(2)	0
M1	0.0045(3)	0.0050(3)	0.0044(3)	0	0.0009(2)	0
Si	0.0051(1)	0.0065(1)	0.0054(2)	−0.0002(1)	0.0013(1)	−0.0004(1)
O1	0.0052(3)	0.0120(3)	0.0112(4)	0.0002(2)	0.0015(3)	−0.0022(3)
O2	0.0126(3)	0.0074(3)	0.0108(3)	−0.0019(2)	0.0030(3)	−0.0006(2)
O3	0.0080(3)	0.0119(3)	0.0071(3)	0.0009(2)	0.0025(3)	−0.0025(2)

clinopyroxene structures, Rossi (1983) and Rossi et al. (1983) adopted the averaged structural parameters for *P*2/*n* pyroxenes, since it is always possible to obtain one extrapolated "mean" *C*2/*c* structural parameter from the corresponding two in the *P*2/*n* structure. Based on this, Rossi et al. (1983) found that, with increasing mean <M1-O> distance from jadeite to diopside, the mean tetrahedral <Si-O> distance increases, whereas the O3-O3-O3 angle of the tetrahedral chain decreases systematically. Our data, as shown in Figures 3 and 4, fall well on these trends. Nevertheless, Figure 4 clearly shows that the O3-O3-O3 angles of *P*2/*n* pyroxenes are not only all smaller than would be expected from a linear extrapolation of the O3-O3-O3 angles between the diopside and jadeite end-members, but they are also more scattered than those of *C*2/*c* pyroxenes, due probably to various degrees of cation ordering in *P*2/*n* clinopyroxenes.

Disordered Si^{4+} and Mg^{2+} in an octahedral site is not common (see Finger and Hazen 1991 for a review) and little is known on the limitations for such substitutions without causing a phase transition. In fact, the strong ordering between $^{VI}Si^{4+}$ and Mg^{2+} into nonequivalent octahedral sites has been thought to be the primary driving force for structural transformations from cubic to tetragonal (majorite-type) garnets (e.g., Takéuchi et al. 1982; Kato and Kumazawa 1985; Fujino et al. 1986; Sawamoto 1987; Angel et al. 1989; Griffen et al. 1992; Hazen et al. 1994; Nakatsuka et al. 1999) and from *C*2/*c* to *P*2/*n* clinopyroxene (Angel et al. 1988). Angel et al. (1989) reported a tetragonal $I4_1/a$ $MgSiO_3$ garnet synthesized at 17 GPa and 1800 °C, in which there are two octahedral sites, one with a composition of $(Mg_{0.2}Si_{0.8})$ and the other with $(Mg_{0.8}Si_{0.2})$. A more ^{VI}Si-Mg disordered case was later found in the *C*2/*c* $(Ca_{0.36}Na_{0.56}Mg_{0.08})(Mg_{0.73}Si_{0.27})Si_2O_6$ clinopyroxene (Yang and Konzett 2005). With the occupation of more than two types of cations in an octahedral site, the ^{VI}Si content can be even higher. This was documented by Nakatsuka et al. (1999) in a majorite $Mg_3{}^{VI}(Mg_{0.32}Si_{0.32}Al_{0.36})_2Si_3O_{12}$ and by Gasparik et al. (2000) in $(K_{0.56}Na_{0.32})(Ca_{0.04}Mg_{1.66}Fe^{2+}_{0.3})^{VI}(Mg_{0.16}Fe^{3+}_{0.05}Al_{0.44}Si_{0.35})_6O_{12}$. Together with our data for the J3 sample,

TABLE 5. Selected bond distances (Å) and angles in clinopyroxenes with six-coordinated Si

Sample	J1	J2	J3	J4	J5	Jadeite*
M2-O1(1) ×2	2.334(1)	2.334(2)	2.351(1)	2.354(1)	2.353(1)	2.360
M2-O2(1) ×2	2.338(1)	2.341(2)	2.397(1)	2.402(1)	2.405(1)	2.414
M2-O3(1) ×2	2.674(1)	2.673(2)	2.773(1)	2.763(1)	2.755(1)	2.741
M2-O3(2) ×2	2.349(1)	2.349(2)	2.382(1)	2.379(1)	2.373(1)	2.366
Average	2.424	2.424	2.476	2.474	2.472	2.470
V	23.325	23.311	24.781	24.753	24.673	24.615
M2(1)-O1(2) ×2	2.394(2)	2.386(2)				
M2(1)-O2(2) ×2	2.433(1)	2.429(2)				
M2(1)-O3(2) ×2	2.921(1)	2.901(2)				
M2(1)-O3(1) ×2	2.441(2)	2.433(2)				
Average	2.547	2.537				
V	26.871	26.581				
M1-O1(1) ×2	2.219(1)	2.199(2)	2.014(1)	2.009(1)	2.004(1)	1.995
M1-O1(2) ×2	2.088(1)	2.076(2)	1.950(1)	1.947(1)	1.945(1)	1.938
M1-O2(2) ×2	1.987(1)	1.977(2)	1.872(1)	1.867(1)	1.862(1)	1.853
Average	2.098	2.084	1.945	1.941	1.937	1.929
V	11.722	11.521	9.607	9.548	9.489	9.368
OAV	107.16	101.428	48.055	47.579	47.058	47.843
OQE	1.0353	1.0332	1.0152	1.0150	1.0149	1.0151
M1(1)-O1(1) ×2	1.825(1)	1.831(2)				
M1(1)-O1(2) ×2	1.822(1)	1.833(2)				
M1(1)-O2(1) ×2	1.774(1)	1.775(2)				
Average	1.807	1.813				
V	7.820	7.892				
PAV	13.892	15.493				
PQE	1.0042	1.0047				
Si1-O1(1)	1.636(1)	1.633(2)	1.635(1)	1.635(1)	1.635(1)	1.636
Si1-O2(1)	1.614(1)	1.613(2)	1.595(1)	1.596(1)	1.595(1)	1.594
Si1-O3(1)	1.621(1)	1.621(2)	1.631(1)	1.632(1)	1.631(1)	1.632
Si1-O3(2)	1.630(1)	1.624(2)	1.644(1)	1.643(1)	1.641(1)	1.637
Average	1.625	1.623	1.626	1.626	1.626	1.625
V	2.186	2.176	2.192	2.191	2.188	2.183
PAV	21.050	20.811	20.590	21.335	22.001	23.026
PQE	1.0054	1.0053	1.0049	1.0051	1.0053	1.0055
Si2-O1(2)	1.639(1)	1.637(2)				
Si2-O2(2)	1.574(1)	1.572(2)				
Si2-O3(2)	1.639(1)	1.638(2)				
Si2-O3(1)	1.658(1)	1.656(2)				
Average	1.628	1.626				
V	2.193	2.186				
PAV	26.837	26.122				
PQE	1.0062	1.0060				
Si1-O3(1)-Si2	133.54(8)	133.87(11)	139.41(7)	139.20(6)	139.11(5)	139.11
Si1-O3(2)-Si2	147.10(8)	146.46(11)				
O3(1)-O3(2)-O3(1)	170.6	171.0	174.3	174.3	174.4	174.67

* Data for jadeite are from McCarthy et al. (2008).

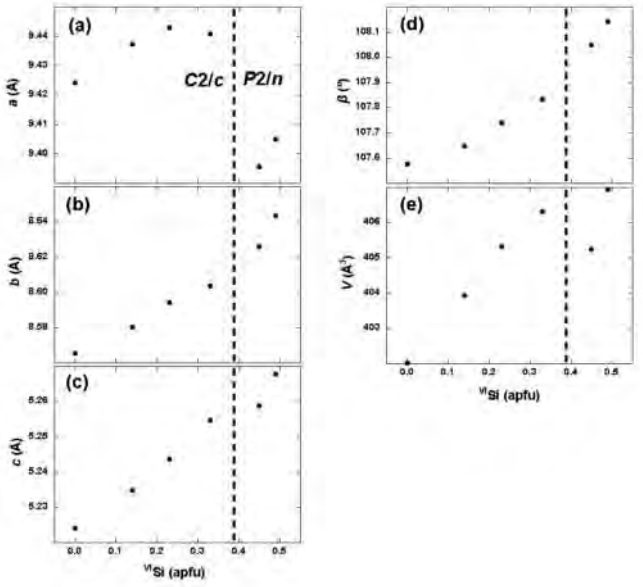

FIGURE 2. Variations of unit-cell parameters of clinopyroxenes in the jadeite-NaPx system as a function of the ^{VI}Si content. The data for jadeite (^{VI}Si = 0) are from McCarthy et al. (2008). Errors (1σ) are smaller than the symbols.

which has an M1 composition ($Mg_{0.37}Si_{0.33}Al_{0.30}$) and shows an evident precursor for the onset of a phase transition, we conclude that the maximum ^{VI}Si content allowed for an Mg/Al dominated octahedral site should be close to ~35%. Above this amount, ^{VI}Si and Mg/Al are likely to occupy distinct sites.

There have been numerous investigations on a variety of pyroxenes with Raman spectroscopy (e.g., Sharma et al. 1983; McMillan 1984; Dowty 1987a, 1987b; Mernagh and Hoatson 1997; Ross and Reynard 1999; Huang et al. 2000; Wang et al. 2001; Zhang et al. 2002; Pommier et al. 2003, 2008; Gatta et al. 2005; Makreski et al. 2006). Yet, there is no detailed Raman spectroscopic study on clinopyroxenes with *P*2/*n* symmetry or containing ^{VI}Si, although *P*2/*n* and *C*2/*c* pyroxenes in the jadeite-augite join have been examined by Boffa Ballaran et al. (1998b) using infrared spectroscopy. In general, the Raman spectra of pyroxenes can be classified into four regions (Zhang et al. 2002 and references therein). Region 1 includes the bands between 800 and 1200 cm^{-1}, which are assigned to Si-O stretching vibrations related to the Si-O_{nb} bonds in the SiO_4 tetrahedra (O_{nb} represents the non-bridging O atom). Region 2 is between 630–800 cm^{-1}. The bands in this region are attributed to the Si-O_{br}-Si vibrations within the silicate chains (O_{br} represents the bridging O atom). Region 3, from 400 to 630 cm^{-1}, includes the bands that are mainly associated with the O-Si-O bending modes of SiO_4 tetrahedra. The bands in region 4, which spans from 50 to 400 cm^{-1}, are of complex nature, chiefly due to lattice modes involving M-O interactions, as well as possible O-Si-O bending. Generally, there may be variations in the relative intensities of the Raman bands with changes in crystal orientation, but there are no observable changes in their wavenumbers (e.g., Mernagh and Hoatson 1997; Huang et al. 2000; Liermann et al. 2006). Therefore, the number of Raman bands observed and their relative widths are a useful indication of structural changes with chemistry or atomic order-disorder (Mernagh and Hoatson 1997; Ross and Reynard 1999; Wang et al. 2001; Zhang et al. 2002; Pommier et al. 2003, 2008; Gatta et al. 2005; Liermann et al. 2006).

Plotted in Figure 5 are Raman spectra of six clinopyroxenes in the jadeite-NaPx system. A comparison of these spectra reveals that the *C*2/*c*-*P*2/*n* transition occurring between ^{VI}Si = 0.33 and 0.45 apfu is characterized by the splitting of many observable Raman bands in the *C*2/*c* structure into doublets in the *P*2/*n* structure, especially for bands in regions 1 and 4. This is consistent with the doubled number of independent atomic sites in the *P*2/*n* structure relative to that in the *C*2/*c* structure. Such splitting becomes more pronounced with increasing ^{VI}Si content. Similar band splitting stemming from the reduction of the symmetry from *C*2/*c* to *P*2/*n* was also observed from the infrared spectra measured on clinopyroxenes in the jadeite-augite system (Boffa Ballaran et al. 1998). For our *C*2/*c* clinopyroxenes, all Raman bands become progressively broader with the increased substitution of (Si^{4+} + Mg^{2+}) for Al^{3+}, indicating the amplified local heterogeneities or positional disorder of atoms as

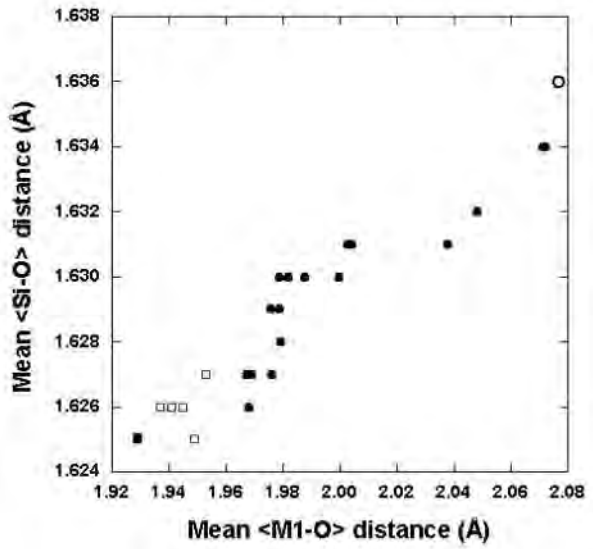

FIGURE 3. The mean <M1-O> distance vs. the mean <Si-O> distance for clinopyroxenes in the jadeite-NaPx and jadeite-diopside systems. The data for jadeite (solid square), diopside (open circle), jadeite-NaPx solid solutions (open squares), and jadeite-diopside solid solutions are from McCarthy et al. (2008), Levien and Prewitt (1981), this study, and Rossi et al. (1983), respectively.

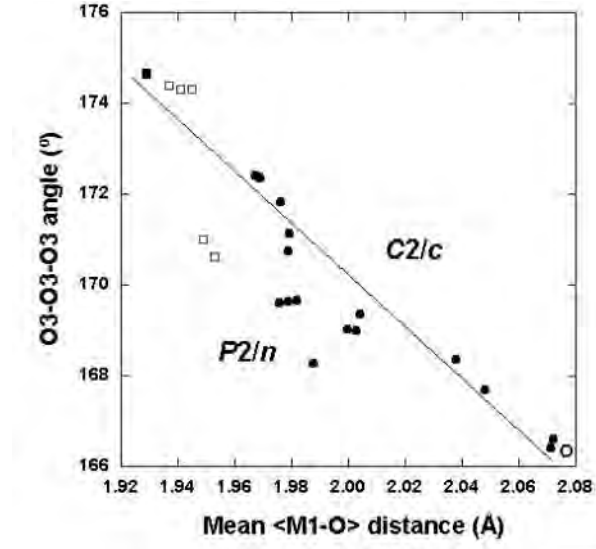

FIGURE 4. The mean <M1-O> distance vs. the O3-O3-O3 angle for clinopyroxenes in the jadeite-NaPx and jadeite-diopside systems. The data symbols are the same as those in Figure 2. Note that all data for *C*2/*c* clinopyroxenes are above the straight line and those for *P*2/*n* ones below it. Errors (1σ) are smaller than the symbols.

the difference in the sizes and charges of M1 cations increases. The increased atomic isotropic displacement parameters (U_{eq}) with increasing ^{VI}Si content for *C*2/*c* clinopyroxenes (Table 5) provides additional support for this inference.

Another notable feature of Figure 5 is the emergence of some Raman bands, such as those at ~340, 596, and 1110 cm^{-1}, with the addition of ^{VI}Si into the *C*2/*c* clinopyroxene structure. Whereas the relative intensities of these bands increase substantially with more replacement of Al^{3+} by (Si^{4+} + Mg^{2+}), their frequencies do not seem to change much, even across the *C*2/*c*-to-*P*2/*n* transition. Hence, these bands are attributable to the presence of ^{VI}Si in clinopyroxenes. In comparison with the Raman spectra for stishovite (Hemley et al. 1986) and majorite (Hofmeister et al. 2004), both of which contain SiO_6 octahedra, we ascribe the band at ~340 cm^{-1} to the SiO_6 octahedral rotation mode and that at ~595 cm^{-1} to the internal O-^{VI}Si-O bending vibration. The band at ~1110 cm^{-1} may rise from the so-called coupling phenomena (Hofmeister et al. 2004)—the corner-sharing between SiO_6 octahedra and SiO_4 tetrahedra making the asymmetric stretch of the SiO_4 tetrahedra become a combined breathing motion of the two polyhedra.

The major Raman bands between 620 and 720 cm^{-1} in pyroxenes are regarded as originating from the symmetric bending vibrations of the O_{br} atoms between adjacent SiO_4 tetrahedra (i.e., Si-O_{br}-Si bending). In general, pyroxenes with one distinct chain, such as those with *C*2/*c* symmetry, exhibit only one major band in this region, whereas pyroxenes with two kinds of chains (such as those with $P2_1/c$ or *Pbca* symmetry) may or may not display a doublet (e.g., Huang et al. 2000; Wang et al. 2001). The doublet has been widely used to distinguish different symmetries of pyroxenes (e.g., Mernagh and Hoatson 1997; Wang et al. 2001; Makreski et al. 2006) or to probe the phase transitions in pyroxenes as a function of pressure, temperature, or composition (e.g., Ross and Reynard 1999; Yang et al. 1999; Ulmer and Stalder 2001; Zhang et al. 2002; Lin 2003, 2004; Pommier et al. 2003, 2008; Gatta et al. 2005). In *P*2/*n* clinopyroxenes, there exist two nonequivalent Si-O_{br}-Si configurations (or two distinct SiO_4 tetrahedra), though there is only one type of crystallographically independent silicate chain. For NaPx (the J1 sample), these two configurations are Si1-O3(1)-Si2 and Si1-O3(2)-Si2, with bond angles of 133.5 and 147.1°, respectively. However, we observed only one strong band at 696 cm^{-1} for this sample (regardless of the crystal orientation). The recorded Raman spectra of omphacite (Kunz et al. 2002; Zhang et al. 2005, 2006) shows only one single strong band at ~675 cm^{-1} as well. Thus, the two Si-O_{br}-Si bending vibrations in *P*2/*n* clinopyroxenes may be actually coupled, since both of them involve the motions of the same Si1 and Si2 atoms.

CONCLUDING REMARKS

Several high-pressure, Na-bearing compounds containing ^{VI}Si have been characterized structurally, such as $Na_2Si(Si_2O_7)$ (Fleet and Henderson 1995), $Na_{1.8}Ca_{1.1}Si_6O_{14}$ (Gasparik et al. 1995), $Na_6Si_3(Si_9O_{27})$ (Fleet 1996), $Na_8Si(Si_6O_{18})$ (Fleet 1998), $Na_2Mg_{4+x}Fe^{3+}_{2-2x}Si_{6+x}O_{20}$ (Gasparik et al. 1999), $(K,Na)_{0.9}(Mg, Fe)_2(Mg, Fe, Al, Si)_6O_{12}$ (Gasparik et al. 2000), as well as the $Na(Mg_xSi_xAl_{1-2x})Si_2O_6$ solid solutions ($0 \le x \le 0.5$) (this study). Not only have these new structure data greatly enriched our knowledge of crystal chemistry in general, but also extended our understanding of the high-pressure behavior of alkali-bearing structures in particular. As pyroxenes are known to invert to majoritic garnets at high pressures and garnets formed in the mantle eclogitic systems become progressively depleted in Al and enriched in Si, M^{2+} (i.e., Mg, Fe, Ca), and Na with increasing pressure (e.g., Gasparik 1989; Bobrov et al. 2008a, 2008b), one may postulate the existence of some high-pressure Na-bearing garnets transformed from the jadeite-NaPx solid solu-

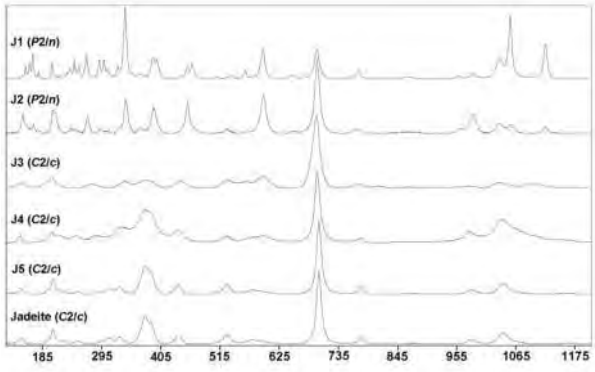

FIGURE 5. Raman spectra of clinopyroxenes in the jadeite-NaPx system.

tions $[Na(Mg_xSi_xAl_{1-2x})Si_2O_6]$ and/or $(Ca_{0.36}Na_{0.56}Mg_{0.08})(Mg_{0.73}Si_{0.27})Si_2O_6$ clinopyroxene (Yang and Konzett 2005). Indeed, a garnet-type polymorph of NaPx, $(Na_2Mg)Si_2(SiO_4)_3$, has been synthesized at 15.4–16.5 GPa and 1650 °C (Gasparik 1989; Pacalo et al. 1992). More interestingly, the reported $NaPx_{16}En_{84}$ inclusion in diamond (Wang and Sueno 1996) was found to have the garnet structure (Wang and Gasparik 2000), implying that appropriate compositions exist in the mantle to stabilize NaPx as a component in pyroxene below the pyroxene-garnet transition pressure, which is approximately 16.5 GPa (Gasparik 1989). Conceivably, as we further explore temperature-pressure-composition space, many other exotic phases containing ^{VI}Si will be discovered and a combination of structure determination/refinements with spectroscopic measurements will undoubtedly lead us to a better understanding of the crystal chemistry of high-pressure phases.

ACKNOWLEDGMENTS

We gratefully acknowledge the support of this study from the Austrian Science Foundation (Grant no. P17845-N10), NSF (EAR-0609906), and the RRUFF project.

REFERENCES CITED

Angel, R.J., Gasparik, T., Ross, N.L., Finger, L.W., Prewitt, C.T., and Hazen, R.M. (1988) A silica-rich sodium pyroxene phase with six-coordinated silicon. Nature, 335, 156–158.

Angel, R.J., Finger, L.W., Hazen, R.M., Kanzaki, M., Weidner, D.J., Liebermann, R.C., and Veblen, D.R. (1989) Structure and twinning of single-crystal $MgSiO_3$ garnet synthesized at 17 GPa and 1800 °C. American Mineralogist, 74, 509–512.

Bobrov, A.V., Kojitani, H., Akaogi, M., and Litvin, Y.A. (2008a) Phase relations on the diopside–jadeite–hedenbergite join up to 24 GPa and stability of Na-bearing majoritic garnet. Geochimica et Cosmochimica Acta, 72, 2392–2408.

Bobrov, A.V., Litvin, Y.A., Bindi, L., and Dymshits, A.M. (2008b) Phase relations and formation of sodium-rich majoritic garnet in the system $Mg_3Al_2Si_3O_{12}$–$Na_2MgSi_5O_{12}$ at 7.0 and 8.5 GPa. Contributions to Mineralogy and Petrology, 156, 243–257.

Boffa Ballaran, T. and Domeneghetti, M.C. (1996) Crystal-chemistry and order parameters of Sesia-Lanzo and Dora-Maira omphacites. Bollettino del Museo Regionale di Scienze Naturali, Supplemento al Volume 13, 273–292.

Boffa Ballaran, T., Carpenter, M.A., Domeneghetti, M.C., and Tazzoli, V. (1998a) Structural mechanisms of solid solution and cation ordering in augite-jadeite pyroxenes: I. A macroscopic perspective. American Mineralogist, 83, 419–433.

——— (1998b) Structural mechanisms of solid solution and cation ordering in augite-jadeite pyroxenes: I. A microscopic perspective. American Mineralogist, 83, 434–443.

Carpenter, M.A., Domeneghetti, M.C., and Tazzoli, V. (1990a) Application of Landau theory to cation ordering in omphacite; 1, Equilibrium behaviour. European Journal of Mineralogy, 2, 7–18.

——— (1990b) Application of Landau theory to cation ordering in omphacite; 2, Kinetic behaviour. European Journal of Mineralogy, 2, 19–28.

Curtis, L., Gittins, J., Kocman, V., Rucklidge, J.C., Hawthorne, F.C., and Ferguson, R.B. (1975) Two crystal structure refinements of a *P*2/*n* titanian ferro-omphacite. Canadian Mineralogist, 13, 62–67.

Day, H.W. and Mulcahy, S.R. (2007) Excess silica in omphacite and the formation of free silica in eclogite. Journal of Metamorphic Geology, 25, 37–50.

Dowty, E. (1987a) Vibrational interactions of tetrahedra in silicate glasses and crystals. I. Calculations on ideal silicate-aluminate-germanate structural units. Physics and Chemistry of Minerals, 14, 80–93.

——— (1987b) Vibrational interactions of tetrahedra in silicate glasses and crystals II. Calculations on melities, pyroxenes, silica polymorphs and feldspars. Physics and Chemistry of Minerals, 14, 122–138.

Finger, L.W. and Hazen, R.M. (1991) Crystal chemistry of six-coordinated silicon: A key to understanding the Earth's deep interior. Acta Crystallographica, B47, 561–580.

Fleet, M.E. (1996) Sodium tetrasilicate: A complex high-pressure framework silicate ($Na_6Si_3[Si_9O_{27}]$). American Mineralogist, 83, 618–624.

——— (1998) Sodium heptasilicate: A high-pressure silicate with six-membered rings of tetrahedra interconnected by SiO_6 octahedra: $[Na_8Si(Si_6O_{18})]$. American Mineralogist, 83, 618–624.

Fleet, M.E. and Henderson, G.S. (1995) Sodium trisilicate—a new high-pressure silicate structure $[Na_2Si(Si_2O_7)]$. Physics and Chemistry of Minerals, 22, 383–386.

Fujino, K., Momoi, H., Sawamoto, H., and Kumazawa, M. (1986) Crystal structure and chemistry of $MnSiO_3$ tetragonal garnet. American Mineralogist, 71, 781–785.

Gasparik, T. (1989) Transformation of enstatite-diopside-jadeite pyroxenes to garnet. Contributions to Mineralogy and Petrology, 102, 389–405.

Gasparik, T., Parise, J.B., Eiben, B.A., and Hriljac, J.A. (1995) Stability and structure of a new high-pressure silicate, $Na_{1.8}Ca_{1.1}Si_6O_{14}$. American Mineralogist, 80, 1269–1276.

Gasparik, T., Parise, J.B., Reeder, R.J., Young, V.G., and Wilford, W.S. (1999) Composition, stability, and structure of a new member of the aenigmatite group, $Na_2Mg_{4+x}Fe^{3+}_{2-2x}Si_{6+x}O_{20}$, synthesized at 13–14 GPa. American Mineralogist, 84, 257–266.

Gasparik, T., Tripathi, A., and Parise, J.B. (2000) Structure of a new Al-rich phase, $[K, Na]_{0.9}[Mg, Fe]_2[Mg, Fe, Al, Si]_6O_{12}$, synthesized at 24 GPa. American Mineralogist, 85, 613–618.

Gatta, G.D., Boffa Ballaran, T., and Iezzi, G. (2005) High-pressure X-ray and Raman study of a ferrian magnesian spodumene. Physics and Chemistry of Minerals, 32, 132–139.

Griffen, D.T., Hatch, D.M., Phillips, W.R., and Kulaksiz, S. (1992) Crystal chemistry and symmetry of a birefringent tetragonal $pyralspite_{75}$-$grandite_{25}$ garnet. American Mineralogist, 77, 399–406.

Hazen, R.M., Downs, R.T., Finger, L.W., Conrad, P.G., and Gasparik, T. (1994) Crystal chemistry of Ca-bearing majorite. American Mineralogist, 79, 581–584.

Hemley, R.J., Mao, H.-K., and Chao, E.C.T. (1986) Raman spectrum of natural and synthetic stishovite. Physics and Chemistry of Minerals, 13, 285–290.

Hofmeister, A., Giesting, P., Wopenka, B., Gwanmesia, G., and Jolliff, B. (2004) Vibrational spectroscopy of pyrope-majorite garnets: Structural implications. American Mineralogist, 89, 132–146.

Huang, E., Chen, C.H., Huang, T., Lin, E.H., and Xu, J. (2000) Raman spectroscopic characteristics of Mg-Fe-Ca pyroxenes. American Mineralogist, 85, 473–479.

Katerinopoulou, A., Katerinopoulos, A., Bieniok, A., Konp, E., Magganas, A., and Amthauer, G. (2007) Crystal chemistry, structure analyses and phase transition experiment on an omphacite from eclogitic metagabbro from Syros island, Greece. Mineralogy and Petrology, 91, 117–128.

Kato, T. and Kumazawa, M. (1985) Garnet phase of $MgSiO_3$ filling the pyroxeneilmenite gap at very high temperature. Nature, 316, 803–805.

Kunz, M., Gillet, P., Fiquet, G., Sautter, V., Graafsma, H., Conrad, P., and Harris, J. (2002) Combined in situ X-ray diffraction and Raman spectroscopy on majoritic garnet inclusions in diamonds. Earth and Planetary Science Letters, 198, 485–493.

Levien, L. and Prewitt, C.T. (1981) High-pressure structural study of diopside. American Mineralogist, 66, 315–323.

Liermann, H.P., Downs, R.T., and Yang, H. (2006) Site disorder revealed through Raman spectra from oriented single crystals: A case study on karooite ($MgTi_2O_5$). American Mineralogist, 91, 790–793.

Lin, C.C. (2003) Pressure-induced metastable phase transition in orthoenstatite ($MgSiO_3$) at room temperature: a Raman spectroscopic study. Journal of Solid State Chemistry, 174, 403–411.

——— (2004) Pressure-induced polymorphism in enstatite ($MgSiO_3$) at room temperature: Clinoenstatite and orthoenstatite. Journal of Physics and Chemistry of Solids, 65, 913–921.

Makreski, P., Jovanovski, G., Gajovic, A., Biljan, T., Angelovski, D., and Jaci-

movic, R. (2006) Minerals from Macedonia. XVI. Vibrational spectra of some common appearing pyroxenes and pyroxenoids. Journal of Molecular Structure, 788, 102–114.
Matsumoto, T., Tokonami, M., and Morimoto, N. (1975) The crystal structure of omphacite. American Mineralogist, 60, 634–641.
McCarthy, A.C., Downs, R.T., and Thompson, R.M. (2008) Compressibility trends of the clinopyroxenes, and in situ high-pressure single-crystal X-ray diffraction study of jadeite. American Mineralogist, 93, 198–209.
McMillan, P. (1984) Structural studies of silicates glasses and melts—applications and limitations of Raman spectroscopy. American Mineralogist, 69, 622–644.
Mernagh, T.P. and Hoatson, D.M. (1997) Raman spectroscopic study of pyroxene structures from the Munni Munni layered intrusion, Western Australia. Journal of Raman Spectroscopy, 28, 647–658.
Mottana, A., Rossi, G., Kracher, A., and Kurat, G. (1979) Violan revisited: Mn-bearing omphacite and diopside. Tschermaks Mineralogische und Petrographische Mitteilungen, 26, 187–201.
Nakatsuka, A., Yoshiasa, A., Yamanaka, T., Ohtaka, O., Katsura, T., and Ito, E. (1999) Symmetry change of majorite solid-solution in the system $Mg_3Al_2Si_3O_{12}$-$MgSiO_3$. American Mineralogist, 84, 1135–1143.
Pacalo, R.E.G., Weidner, D.J., and Gasparik, T. (1992) Elastic properties of sodium-rich majorite garnet. Geophysical Research Letters, 19, 1895–1898.
Pavese, A., Bocchio, R., and Ivaldi, G. (2000) In situ high temperature single crystal X-ray diffraction study of a natural omphacite. Mineralogical Magazine, 64, 983–993.
Pommier, C.J.S., Denton, M.B., and Downs, R.T. (2003) Raman spectroscopic study of spodumene ($LiAlSi_2O_6$) through the pressure-induced phase change from *C*2/*c* to *P*2_1/*c*. Journal of Raman Spectroscopy, 34, 769–775.
Pommier, C.J.S., Redhammer, G.J., Denton, M.B., and Downs, R.T. (2008) Raman spectroscopic and visible absorption investigation of $LiCrSi_2O_6$ pyroxene under pressure. Applied Spectroscopy, 62, 766–772.
Robinson, K., Gibbs, G.V., and Ribbe, P.H. (1971) Quadratic elongation, a quantitative measure of distortion in coordination polyhedra. Science, 172, 567–570.
Ross, N.L. and Reynard, B. (1999) The effect of iron on the *P*2_1/*c* to *C*2/*c* transition in (Mg,Fe)SiO_3 clinopyroxenes. European Journal of Mineralogy, 11, 585–589.
Rossi, G. (1983) A review of the crystal chemistry clinopyroxenes in eclogites and eclogite-facies rocks. In D.C. Smith, Ed., Eclogites and Eclogite-Facies Rocks, p. 237–270. Elsevier, Amsterdam.
Rossi, G., Tazzoli, V., and Ungaretti, L. (1981) Crystal-chemical studies on sodic clinopyroxenes. Proceedings of the XI General Meeting of IMA, Rock-forming Minerals, p. 20–45.
Rossi, G., Smith, D.C., Ungaretti, L., and Domeneghetti, C. (1983) Crystal-chemistry and cation ordering in the system diopside-jadeite: A detailed study by crystal structure refinement. Contributions to Mineralogy and Petrology, 83, 247–258.
Sawamoto, H. (1987) Phase diagram of $MgSiO_3$ at pressures up to 24 GPa and temperatures up to 2200 °C: Phase stability and properties of tetragonal garnet. In M.H. Manghnani and Y. Syono, Eds., High-Pressure Research in Mineral Physics, p. 209–219. Terra Scientific Publishing, Tokyo.
Sharma, S.K., Simons, B., and Yoder Jr., H. (1983) Raman study of anorthite, calcium Tschermak's pyroxene, and gehlenite in crystalline and glassy states. American Mineralogist, 68, 1113–1125.
Sheldrick, G.M. (2008) A short history of SHELX. Acta Crystallographica, A64, 112–122.
Takéuchi, Y., Haga, N., Umizu, S., and Sato, G. (1982) The derivative structure of silicate garnets in grandite. Zeitschrift für Kristallographie, 158, 53–99.
Ulmer, P. and Stalder, R. (2001) The Mg(Fe)SiO_3 orthoenstatite-clinoenstatite transitions at high pressures and temperatures determined by Raman-spectroscopy on quenched samples. American Mineralogist, 86, 1267–1274.
Wang, A., Jolliff, B.L., Haskin, L.A., Kuebler, K.E., and Viskupic, K.M. (2001) Characterization and comparison of structural and compositional features of planetary quadrilateral pyroxenes by Raman spectroscopy. American Mineralogist, 86, 790–806.
Wang, W. and Gasparik, T. (2000) Evidence for a deep-mantle origin of a NaPx-En inclusion in diamond. International Geology Review, 42, 1000–1006.
Wang, W. and Sueno, S. (1996) Discovery of a NaPx-En inclusion in diamond: Possible transition zone origin. Mineralogical Journal, 18, 9–16.
Yang, H. and Konzett, J. (2005) Crystal chemistry of a high-pressure *C*2/*c* clinopyroxene with six-coordinated silicon. American Mineralogist, 90, 1223–1226.
Yang, H., Finger, L.W., Conrad, P.G., Prewitt, C.T., and Hazen R.M. (1999) A new pyroxene structure observed at high pressure: Single-crystal X-ray and Raman study of *Pbcn*-*P*2_1*cn* phase transition in protopyroxene. American Mineralogist, 84, 245–256.
Zhang, L., Song, S., Liou, J.G., Ai, Y., and Li, X. (2005) Relict coesite exsolution in omphacite from Western Tianshan eclogites, China. American Mineralogist, 90, 181–186.
Zhang, M., Redhammer, G.J., Salje, E.K.H., and Mookherjee, M. (2002) $LiFeSi_2O_6$ and $NaFeSi_2O_6$ at low temperature: An infrared spectroscopic study. Physics and Chemistry of Minerals, 29, 609–616.
Zhang, Z., Shen, K., Xiao, Y., Hoefs, J., and Liou, J.G. (2006) Mineral and fluid inclusions in zircon of UHP metamorphic rocks from the CCSD-main drill hole: A record of metamorphism and fluid activity. Lithos, 92, 378–398.

Manuscript received September 3, 2008
Manuscript accepted March 6, 2009
Manuscript handled by Martin Kunz